JOURNAL OF THE ROYAL SOCIETY Interface

Adhesion formation of primary human osteoblasts and the functional response of mesenchymal stem cells to 330?nm deep microgrooves

M.J.P Biggs, R.G Richards, S McFarlane, C.D.W Wilkinson, R.O.C Oreffo and M.J Dalby

J. R. Soc. Interface 2008 **5**, 1231-1242
doi: 10.1098/rsif.2008.0035

JOURNAL OF THE ROYAL SOCIETY Interface

J. R. Soc. Interface (2008) **5**, 1231–1242
doi:10.1098/rsif.2008.0035
Published online 18 March 2008

Adhesion formation of primary human osteoblasts and the functional response of mesenchymal stem cells to 330 nm deep microgrooves

M. J. P. Biggs[1,2,*], R. G. Richards[2], S. McFarlane[3], C. D. W. Wilkinson[3,4], R. O. C. Oreffo[5] and M. J. Dalby[1]

[1]*Centre for Cell Engineering, Institute of Biomedical and Life Sciences, Joseph Black Building, University of Glasgow, Glasgow G12 8QQ, UK*
[2]*AO Research Institute, AO Foundation, Clavadelerstrasse 8, 7270 Davos Platz, Switzerland*
[3]*James Watt Nanofabrication Centre, Department of Electronics and Electrical Engineering, Rankine Building, University of Glasgow, Glasgow G12 8QQ, UK*
[4]*Centre for Cell Engineering, Department of Electronics and Electrical Engineering, Rankine Building, University of Glasgow, Glasgow G12 8LT, UK*
[5]*Bone and Joint Research Group, Developmental Origins of Health and Disease, Institute of Developmental Sciences, University of Southampton, Southampton S016 6YD, UK*

The surface microtexture of an orthopaedic device can regulate cellular adhesion, a process fundamental in the initiation of osteoinduction and osteogenesis. Advances in fabrication techniques have evolved to include the field of surface modification; in particular, nanotechnology has allowed for the development of experimental nanoscale substrates for investigation into cell nanofeature interactions. Here primary human osteoblasts (HOBs) were cultured on ordered nanoscale groove/ridge arrays fabricated by photolithography. Grooves were 330 nm deep and either 10, 25 or 100 μm in width. Adhesion subtypes in HOBs were quantified by immunofluorescent microscopy and cell–substrate interactions were investigated via immunocytochemistry with scanning electron microscopy. To further investigate the effects of these substrates on cellular function, 1.7 K gene microarray analysis was used to establish gene regulation profiles of mesenchymal stem cells cultured on these nanotopographies. Nanotopographies significantly affected the formation of focal complexes (FXs), focal adhesions (FAs) and supermature adhesions (SMAs). Planar control substrates induced widespread adhesion formation; 100 μm wide groove/ridge arrays did not significantly affect adhesion formation yet induced upregulation of genes involved in skeletal development and increased osteospecific function; 25 μm wide groove/ridge arrays were associated with a reduction in SMA and an increase in FX formation; and 10 μm wide groove/ridge arrays significantly reduced osteoblast adhesion and induced an interplay of up- and downregulation of gene expression. This study indicates that groove/ridge topographies are important modulators of both cellular adhesion and osteospecific function and, critically, that groove/ridge width is important in determining cellular response.

Keywords: osteoblasts; mesenchymal stem cells; focal adhesions; genomic regulation; nanotopography; nanobioscience

1. INTRODUCTION

The cell–biomaterial interface functions not only to define the boundary between tissue and implant, but also as a mediator of first stage protein interactions as well as later stage cell-specific adhesion and orientation. Functional modification of the cell–substrate interface is now recognized as a necessary process in orthopaedic design for successful integration and performance of a device *in vivo*, the paradigm of such being biomaterial-mediated regulation of osseoinduction and osteospecific function.

The phenomenon of cellular contact guidance on grooved topography has been well documented in literature (Den Braber *et al.* 1998; Karuri *et al.* 2004; Lenhert *et al.* 2005). Nanoscale grooves with dimensions similar to those found *in vivo* have been shown to

*Author and address for correspondence: Centre for Cell Engineering, Institute of Biomedical and Life Sciences, Joseph Black Building, University of Glasgow, Glasgow G12 8QQ, UK (m.biggs.1@research.gla.ac.uk).

Received 25 January 2008
Accepted 21 February 2008

cause contact guidance and alignment in studies involving human cell types, including corneal epithelial cells (Teixeira *et al.* 2003), fibroblasts (Dalby *et al.* 2003*b*) and osteoblasts (Lenhert *et al.* 2005).

Bone extracellular tissue is a natural composite biomaterial with a complex hierarchical structure, composed of a macromolecular network including proteins, glycoproteins and polysaccharides, into which mineral phase hydroxyapatite crystals are embedded, providing an environment rich in both biochemical and topographical cues. Macroscopically trabeculae form into struts that are typically orientated along lines of force resulting from mechanical loading. Cortical bone is composed of elongated, cylindrical osteons of approximately 10–500 μm in diameter (Rho *et al.* 1998). Each osteon is a cylinder consisting of multiple concentric lamellae of approximately 3–7 μm in thickness (Giraud-Guille 1988). Collagen fibres within each lamella are arranged into parallel bundles that lie obliquely relative to adjacent lamellae (Rubin *et al.* 2004); in addition, collagen molecules aggregate into highly ordered fibrils, composed of three protein chains, wound together in a triple helix of approximately 300 nm in length (Wagner & Weiner 1992), which also present a banded pattern at the ultrastructural level composed of 69 nm repeat banding units (Brodsky & Persikov 2005; Bozec *et al.* 2005).

Increased knowledge of this intricate extracellular environment, and how cells react within it, has resulted in the development of biomimetic materials to guide morphogenesis in tissue repair and tissue engineering, particularly in the field of topographical modification. Nanotechnology aims to create and use structures and systems in the size range of approximately 0.1–500 nm covering the atomic, molecular and macromolecular length scales.

Cell adhesion is an essential element of many physiological situations, including tissue maintenance, wound healing, development, angiogenesis and cell migration. Focal adhesions (FAs) were initially observed in 1964 (Curtis 1964), and later described by Abercrombie *et al.* (1971) as electron-dense regions along the ventral plasma membrane that make intimate contact with the substratum in cultured cells (Abercrombie *et al.* 1971). These structures play opposing roles in cell motility, aiding both in the generation of cellular strain to generate lamellopodium formation and polarized motility, and as anchoring complexes that resist detachment from the substratum and aid in cellular spreading. A highly ordered hierarchical recruitment of FA-associated proteins occurs during adhesion plaque assembly (Zamir & Geiger 2001). Vinculin is a plasma membrane-associated protein found in adhesion complexes and involved in the coupling of the actin-based microfilaments to the adhesion plaque (Zimerman *et al.* 2004). Vinculin is present in a number of adhesion subtypes and provides a definite detection system for FA sites by means of specific antibody detection.

However, the mechanical response of a cell to its surroundings and the onset of adhesion cannot be accurately described without considering the biochemical and genetic interplays that control signal transduction and protein production. FAs assemble into complex signalling systems where transmembrane integrin receptors transduce signals from the extracellular matrix (ECM) to regulate cellular function and gene expressions, such as cellular growth and differentiation. Work to date has focused on gaining a quantitative understanding of the interconnected mechanical and genetic networks that occur during cell mechanotransduction, specifically those processes that direct osseointegration, matrix deposition and bony tissue neogenesis. Alterations in gene and protein expression can occur within minutes of a cell adhering to a surface. Recently it has been suggested that adhesion complexes may transmit mechanical cues directly to the nucleus through cytoskeletal tension and that this mechanotransduction as well as adhesion kinetics could play a role in topographic induction of cellular differentiation (Dalby *et al.* 2006).

Here photolithography was used to produce three grooved topographies of identical groove depths with different widths (10, 25 and 100 μm repeat width, 330 nm groove depth and 2 cm length). Primary human osteoblasts (HOBs) derived from femoral head and condyle biopsies, and Stro-1 immunoselected human mesenchymal stem cells (MSCs) isolated from the marrow of a femoral diaphysis were used as cell models to investigate morphological and functional response, respectively, to grooved topographies. HOB adhesion complex formation was quantified and cytoskeletal morphology was investigated with scanning electron and fluorescence microscopy. Two extremes of groove width were used for the functional response study—100 and 10 μm groove arrays. This was then followed up with human 1718 gene cDNA microarrays to compare MSC reaction to the grooved topographies with response to a flat surface at 21 days of cell culture. Microarray allowed simultaneous gene detection in planar controls and grooved substrates. Data were then analysed by Ingenuity Pathways Analysis. Interesting changes were observed in the relative level of expression in genes involved in the areas of cell–cell signalling, cytoskeletal formation, ECM remodelling and adhesion-associated signalling.

2. MATERIAL AND METHODS

2.1. Nanopatterning and die fabrication

Samples were made in a three-step process of photolithography, nickel die fabrication and embossing.

2.1.1. Photolithography. Silicon wafers were cleaned under acetone in an ultrasonic bath for 5 min. They were then rinsed thoroughly in reverse osmosis water (ROH_2O) and blow-dried with an air gun. Next, they were spun with primer for 30 s at 4000*g*, then with S1818 photoresist for 30 s at 4000*g* and baked for 30 min at 90°C. The resulting layer was measured to be 1.8 μm thick. The photoresist layer was exposed to UV light through a chrome mask featuring an array of parallel slits on a Karl Suss MA6 mask aligner for 3.8 s. Then the resist layer was developed for 75 s in 50 : 50, Microposit developer: ROH_2O.

The specific design pattern, in this case rectangular slits, was achieved by reactive ion etching using the exposed photoresist as a mask. The silicon substrate was etched in the silicon tetrachloride gas plasma of a Plasmalab System 100 machine (gas flow = 18 sccm, pressure = 9mTorr, rf power = 250 W, DC bias = −300 V). The wafer was etched individually at 7 min at a nominal etch rate of 18 nm min^{-1}. It was then stripped of resist in an acetone ultrasound bath for 5 min, followed by a 5 min soak in concentrated sulphuric acid/hydrogen peroxide mixture before rinsing thoroughly in ROH_2O and drying in an air gun. The two subsequent topographies were 330 nm deep grooves that were 10, 25 or 100 μm in width.

2.1.2. Nickel shim fabrication. To facilitate polymeric replication of the topographical grooves, nickel shims were made directly from the patterned S1818 photoresist samples. A thin (50 nm) layer of Ni-V was sputter coated on both of the samples. That layer acted as an electrode in the subsequent electroplating process. The shims were plated to a thickness of approximately 300 nm (for more information about the procedure see Gadegaard *et al.* (2003)). The shims were finally trimmed to approximately 30×30 mm sizes using a metal guillotine. Imprinting of the nickel shims into poly(methyl-methacrylate) (pMMA) (Goodfellow, UK) was achieved using an Obducat nanoimprinter. Subsequent replicas possessed a nanoimprinted area of 1.5 cm^2. Planar pMMA (average roughness of 1.17 nm over 10 mm^2) was used as a control substrate.

2.2. HOB cell culture

The methodology has been described previously (Biggs *et al.* 2007). Briefly HOBs derived from a femoral head biopsy of an 84-year-old and a knee biopsy of a 74-year-old Caucasian woman (PromoCell, Heidelberg, Germany) were cultured in 75 cm^2 culture flasks. HOBs were expanded to passage 4 following five weeks of culture and were subsequently trypsinized in 0.04% Trypsin/0.03% EDTA (Heidelberg, Germany) and seeded onto untreated experimental substrates. Cells were maintained in PromoCell osteoblast growth medium containing 10% foetal calf serum (FCS; Heidelberg, Germany) that was replaced every 2 days. Following 7 days of culture, the HOBs were maintained for 4 days without changing the medium, inducing a brief period of serum starvation. Osteoblast growth medium encompassing 10% FCS was subsequently introduced to the culture following 4 days of serum starvation and HOBs were allowed to metabolize for 17 hours, giving rise to a population of cells possessing a synchronized nuclear cycle. Following this period, the HOBs were cultured in osteoblast growth medium containing 10 μM 5-bromo-2-deoxyuridine (BrdU) for 3 hours.

MSCs were enriched using Stro-1 antibody and magnetic cell sorting as previously described (Howard *et al.* 2002; Mirmalek-Sani *et al.* 2006), from bone marrow samples obtained from haematologically normal patients undergoing routine hip replacement surgery. These cells represent the adherent bone marrow stromal cell fraction. MSCs were maintained in basal α-minimal essential medium (Invitrogen, Carlsbad, CA, USA) containing 10% FCS that was replaced every 2 days.

2.3. Immunocytochemistry for light microscopy

HOBs on test materials were fixed in 4% paraformaldehyde in phosphate-buffered solution (PBS), with 1% sucrose at 37°C for 15 min. Once fixed, the samples were washed with PBS. Samples were permeabilized with buffered 0.5% Triton X-100 (10.3 g sucrose, 0.292 g NaCl, 0.06 g $MgCl_2$, 0.476 g (4-(2-hydroxyethyl)-1-piperazine-ethanesulphonic acid) (HEPES), 0.5 ml Triton X-100, in 100 ml water; pH 7.2) at 4°C for 5 min. Non-specific binding sites were blocked with 1% bovine serum albumin (BSA) in PBS at 37°C for 5 min and subsequently incubated for 2 hours with a 1 : 200 concentration of anti-vinculin (monoclonal anti-human raised in mouse (clone hVin-1; IgG1); Sigma, Poole, UK), followed by an incubation in 1 : 100 concentration of anti-BrdU/DNase solution for 1 hour (37°C) (RPN2001, Amersham Biosciences cell proliferation kit, Uppsala, Sweden). Simultaneously, rhodamine-conjugated phalloidin was added for the duration of this incubation (1 : 100, Molecular Probes, OR, USA). Non-specific charges (e.g. remaining aldehyde) were neutralized with 0.5% Tween 20/PBS (5×3 min) to minimize background labelling. A secondary biotin-conjugated antibody, (1 : 50 in 1% BSA/PBS, monoclonal horse anti-mouse (IgG), Vector Laboratories, UK) was added for 1 hour (37°C) followed by subsequent washing as mentioned above. Fluorescein isothiocyanate-conjugated streptavidin was added (1 : 50 in 1% BSA/PBS; Vector Laboratories, UK) at 4°C for 30 min, and given a final wash. Samples were mounted in Vectorshield mountant for fluorescence (Vector Laboratories, UK), then viewed with a Zeiss Axiovert 200 M microscope with a Zeiss Plan Neofluor 40× (0.75 NA) lens. Image manipulation in Adobe Photoshop was then used to superimpose the colour channels to show adhesion complexes (vinculin) in green, actin in red and S-phase nuclei in blue.

2.4. Immunocytochemistry for SEM

The immunolabelling method was a modified version of that first described by Richards *et al.* (2001). Briefly, the cells were rinsed for 2 min in 0.1M 1,4 piperazine bis(2-ethanosulphonic acid) (PIPES) buffer (pH 7.4) before being permeabilized with buffered 0.5% Triton X-100 (4×1 min; 10.3 g sucrose, 0.292 g NaCl, 0.06 g $MgCl_2$, 0.476 g HEPES, 0.5 ml Triton X-100, in 100 ml water; pH 7.2) to remove the cell membrane. Cells were then stabilized in 4% paraformaldehyde with 1% sucrose in 0.1 M PIPES, pH 7.4, buffer, for 5 min and rinsed three times for 2 min in 0.1 M PIPES buffer to remove unreacted aldehyde. Non-specific binding sites were blocked with 1% BSA and 0.1% Tween 20 in 0.1 M PIPES buffer, pH7.4, for 15 min. The cells were then incubated with mouse anti-human vinculin (monoclonal anti-human raised in mouse (clone hVin-1; IgG1); Sigma, Poole, UK) diluted 1 : 200 in PIPES

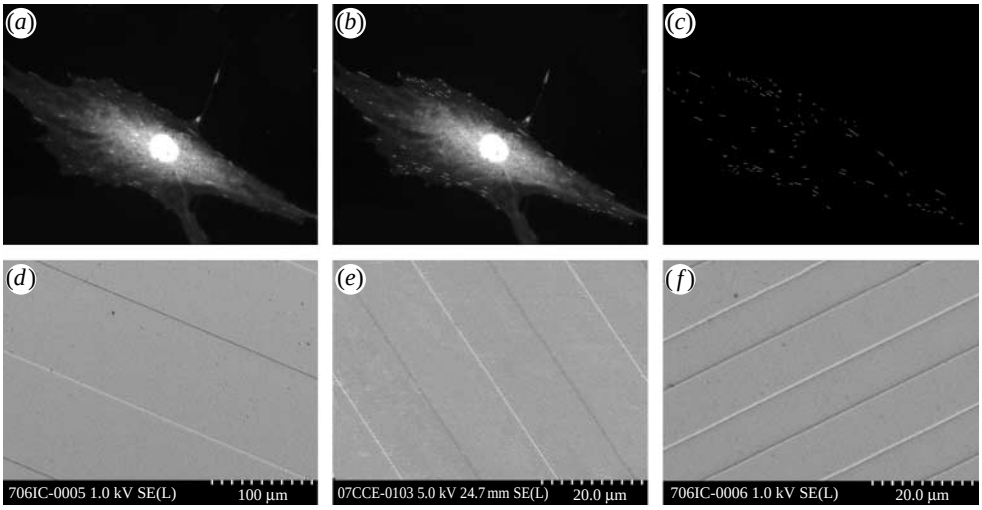

Figure 1. *Adhesion quantification of S-phase HOBs and characterization of experimental substrates.* (*a–c*) Adhesion-associated vinculin was immunolabelled, images were scored with a straight white line, and analysed by image analysis software. Substrates were 330 nm deep and had widths of (*d*) 100 µm, (*e*) 25 µm and (*f*) 10 µm.

buffer +1% BSA+0.1% Tween 20 for 2 hours at 37°C. The cells were rinsed six times for 2 min in PIPES+1% BSA+0.1% Tween 20. Non-specific binding sites were blocked with 5% goat serum+1% BSA+0.1% Tween 20 in PIPES buffer for 15 min. The cells were labelled with goat anti-mouse 5 nm gold conjugate (BBI, Cardiff, UK) diluted 1 : 200 in PIPES buffer+1% BSA +0.1% Tween 20 overnight for 12 hours at 22°C. All samples were then rinsed six times for 2 min in PIPES buffer. The samples were fixed permanently in 2.5% glutaraldehyde for 5 min in PIPES buffer and rinsed three times for 2 min in PIPES buffer. Gold probes were silver enhanced with a silver developing solution for 7 min (BBI, Cardiff, UK). The samples were immediately rinsed two times in ultrapure water to remove any unreacted enhancer. Additional contrasting of the cell was accomplished by staining the cells with 1% osmium tetroxide in PIPES for 1 hour.

2.5. Scanning electron microscopy

The cells were dehydrated through an ethanol series (50, 60, 70, 80, 90, 96 and 100%) followed by a fluorisol/ethanol series (25, 50, 75 and 100%; fluorisol —1,1,2 trichloro,1,2,2, trifluoroethane). The samples were critical point dried (Polaron E3100, Quorum Technologies, UK), mounted on aluminium stubs and coated with a 12 nm layer of carbon using a Baltec CED030 carbon thread evaporator (Baltec, FL, USA). The samples (both with and without cells) were imaged using an Hitachi S-4700 field emission scanning electron microscope fitted with an Autrata yttrium aluminium garnet backscattered electron (BSE) scintillator type detector. The images were taken in both the secondary electron and BSE modes, with accelerating voltages between 2 and 10 kV; the BSE images were taken with an emission current of 50 µA, an aperture of 100 µm (apt1), working distances of 10–12 mm to allow low voltage imaging (Richards & Ap Gwynn 1995).

2.6. Image analysis

Cell images ($n \geq 40$ per substrate) were exported to Adobe Photoshop and adhesion complexes scored with a three-pixel wide straight line on a layer superimposed onto the background image creating an adhesion schematic (figure 1*a–c*). Analysis of individual adhesions ($n \geq 60$ per cell) was performed by Sigma Stat (SSI, San Jose, CA, USA) as previously described (Biggs *et al.* 2006; for more information see Biggs *et al.* (2007)). Criteria for adhesion classification were according to size restrictions described in current literature (Bershadsky *et al.* 1985; Bershadsky *et al.* 2006). Adhesion complexes measuring less than 1 µm in length were assigned as focal complexes (FXs), those from 1 to 5 µm in length were designated as FAs, while those measuring over 5 µm in length were accordingly classified as supermature adhesions (SMAs). Data were sorted into adhesion subtype and analysed using Kruskal–Wallis one-way analysis of variance on ranks, which compared like subtypes. Results of $p < 0.05$ were considered significant (differences of $p < 0.05$ denoted by asterisk, and hash symbol dependent on adhesion subtype).

2.7. RNA isolation and microarray analysis

RNA extraction from confluent layers of MSCs on experimental substrates ($n=5$) and microarray hybridization ($n=5$) was according to the methodology previously described (Dalby *et al.* 2005). Individual gene expression detection was carried out with 1.7 K distinct human transcripts spotted arrays obtained from the Ontario Cancer Institute Microarray Centre. The functional and canonical analyses were generated through the use of Ingenuity Pathways Analysis (Ingenuity Systems, www.ingenuity.com). Changes in gene expression were associated with canonical pathways in the Ingenuity Pathways Knowledge Base. The significance of the association between the dataset and the canonical pathway was measured in two ways. (i) A ratio of the number of genes from the dataset that map to the

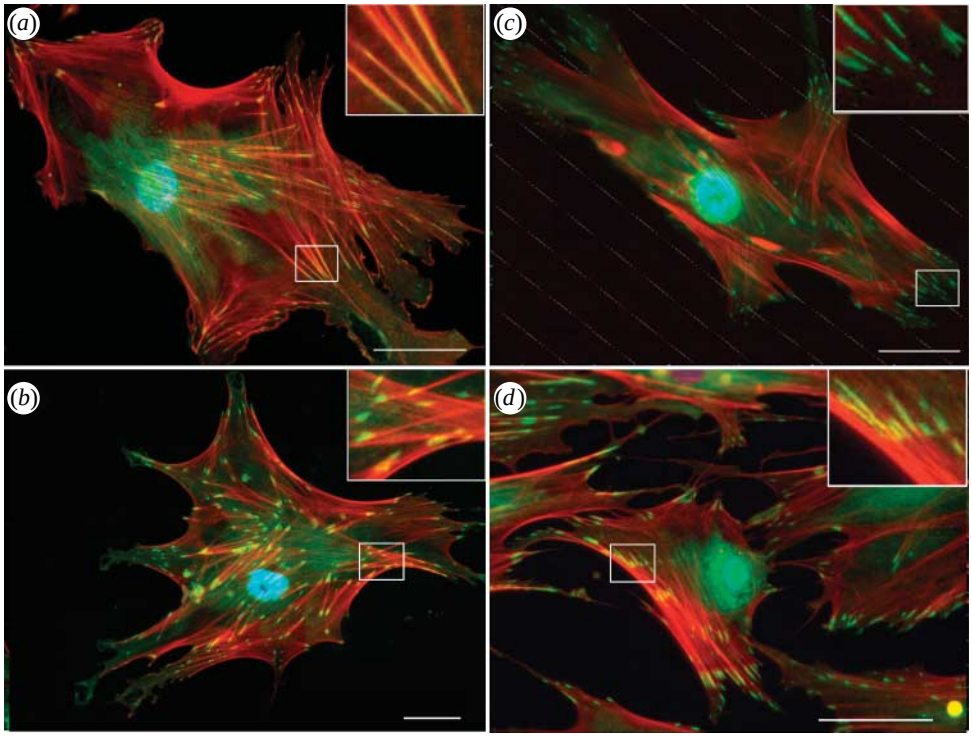

Figure 2. *Tri-fluorescent labelling of adhesion complexes and stress fibre organization in S-Phase HOBs on experimental substrates.* (*a*) HOBs cultured on planar controls formed well-organized stress fibres and numerous SMAs. (*b*) Osteoblasts on 100 µm grooves possessed a well-developed actin cytoskeleton. Adhesions were large and numerous. (*c*) HOBs cultured on 25 µm grooves developed an organized actin cytoskeleton. Adhesion formation was reduced relative to planar controls. (*d*) HOBs cultured on 10 µm groove arrays disrupted cellular spreading. Adhesion formation was influenced by groove orientation. Bar = 50 µm; red, actin; green, vinculin; blue, S-phase nuclei.

pathway divided by the total number of genes that map to the canonical pathway is displayed. (ii) Fischer's exact *t*-test was used to calculate a *p*-value determining the probability that the association between the genes in the dataset and the canonical pathway is explained by chance alone (for more information see Dalby *et al.* 2003*b*)

3. RESULTS

3.1. Nanotopography and substrate characterization

The embossing process resulted in the fabrication of three groove/ridge topographies possessing identical groove depths and periodicity as verified by SEM (figure 1*a–c*). Grooves and ridges were 330 nm deep/high with widths of 10, 25 and 100 µm. Planar controls had an average roughness of 1.17 nm over 10 mm^2.

3.2. HOB morphology and cytoskeletal organization

Nanogroove substrates modified S-phase HOB morphology and cytoskeletal organization relative to controls. HOBs cultured on all experimental substrates experienced increased cellular alignment, which was inversely proportional to groove/ridge width (figures 2–4). Actin cytoskeletal elements in S-phase HOBs on planar controls were prominent and organized into well-developed stress fibres, which typically spanned the entire cell body (figure 2*a*). Stress fibre networks in osteoblasts on 100 µm groove/ridge arrays appeared similar to cells on planar controls. Cells cultured on 25 µm groove/ridge arrays possessed ordered stress fibre organization and also demonstrated actin alignment in the groove direction. Actin fibres in HOBs on 10 µm groove/ridge arrays could be seen to run either perpendicular or parallel to the grooves, but stress fibres arranged both parallel and perpendicular to groove direction rarely occurred in a single cell (figure 2*b–d*). The HOBs on 10 µm groove/ridge topographies adopted a non-spread or a polarized elongated morphology, demonstrating contact guidance (figures 2–4*d*). Cells cultured on all experimental substrates but 10 µm groove/ridge arrays possessed a well-developed microtubule network (figure 3*a–c*). HOBs cultured on 10 µm grooves formed dense microtubule bundles that were orientated in the direction of cell polarity (figure 3*d*).

3.3. Adhesion characterization

Quantification of adhesion distribution by vinculin immunolabelling revealed significant differences in adhesion formation in S-phase HOBs. The HOBs on planar controls formed numerous adhesions of all subtypes. SMAs were located predominantly at the perinuclear region and non-advancing areas of the cell periphery, while FAs and focal complexes were prominent at the region immediately preceding the leading edge and the extreme leading edge, respectively (figures 2*a* and 4*a*). Adhesion formation in HOBs on 100 µm groove/ridge substrates was similar to that

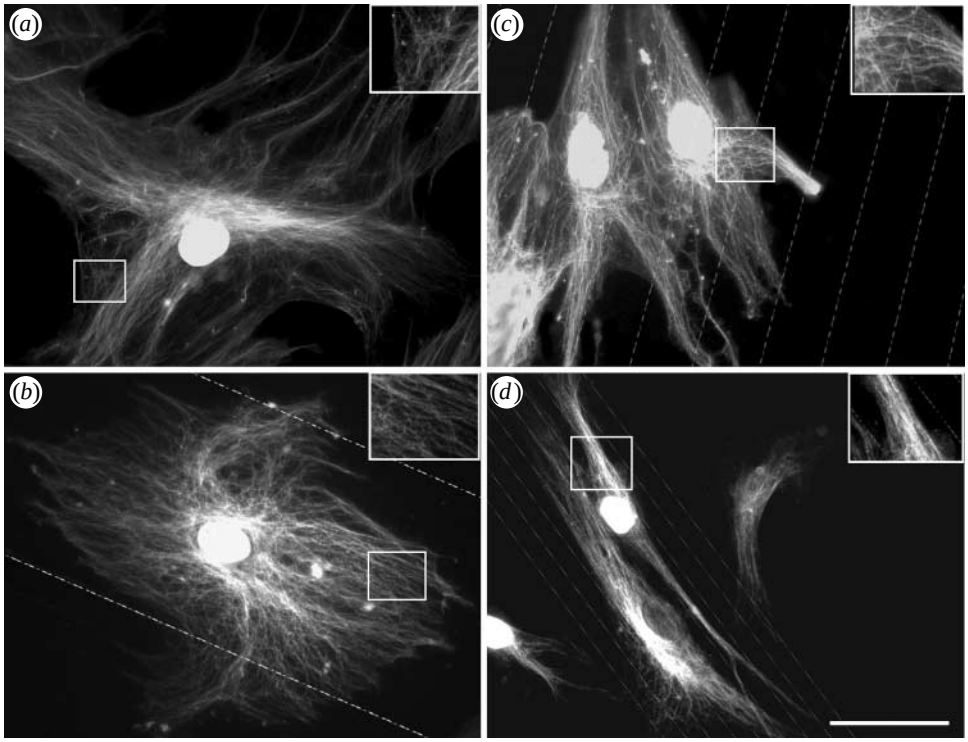

Figure 3. *Dual immunolabelling of the tubulin cytoskeleton and S-phase nuclei of HOBs on experimental substrates.* (*a*,*b*) HOBs cultured on control and 100 µm groove substrates formed organized tubulin networks. Tubulin density decreased with increasing distance from the nucleus. (*c*) HOBs on 25 µm grooves demonstrated increased contact guidance. Cells were less spread and possessed a denser tubulin network. (*d*) Contact guidance was increased in cells on 10 µm groove substrates. S-phase HOBs formed a dense and polarized microtubule network. Bar = 50 µm.

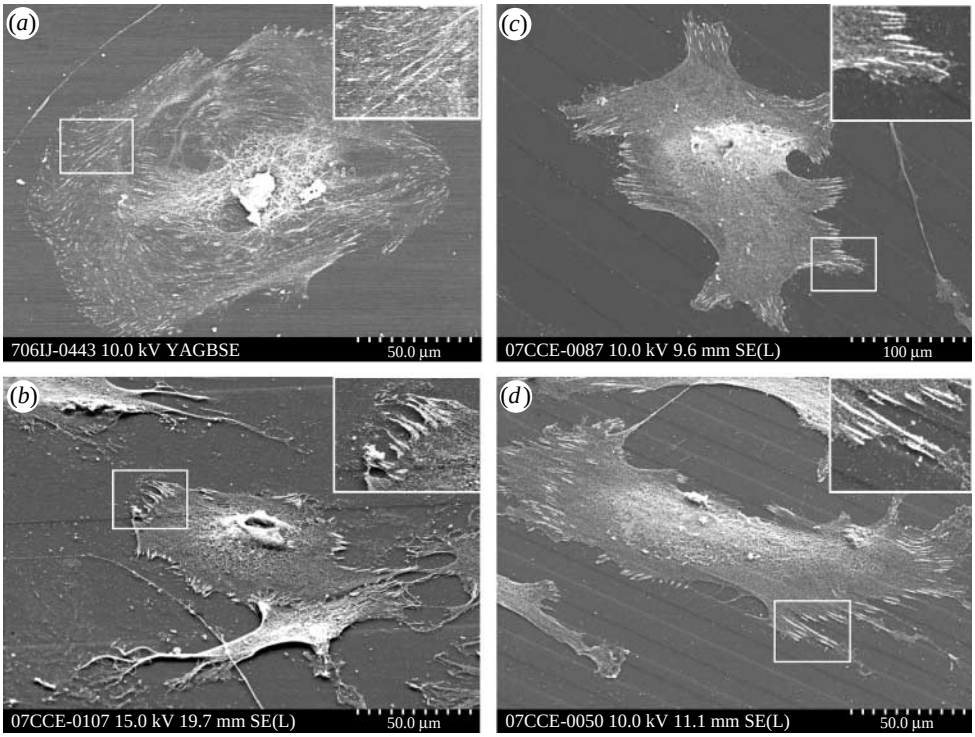

Figure 4. *Scanning electron immunolabelling of adhesion complexes in HOBs on experimental substrates.* (*a*) HOBs cultured on flat pMMA formed numerous focal complexes. (*b*) Diffuse 100 µm grooves did not affect adhesion formation. (*c*) HOBs on 25 µm grooves formed adhesions predominantly on the raised ridge areas (indicated in insert). (*d*) HOBs cultured on 10 µm grooves influenced cellular and adhesion orientation, aligning both HOBs and adhesion complexes with groove direction.

of HOBs on planar controls (figures 2*b* and 4*b*); adhesion location and orientation were not significantly affected by this topography. Orientation and location of adhesions were significantly affected in HOBs on 25 and 10 µm groove/ridge arrays (figure 4*c*,*d*). Adhesion formation occurred predominantly on ridge structures

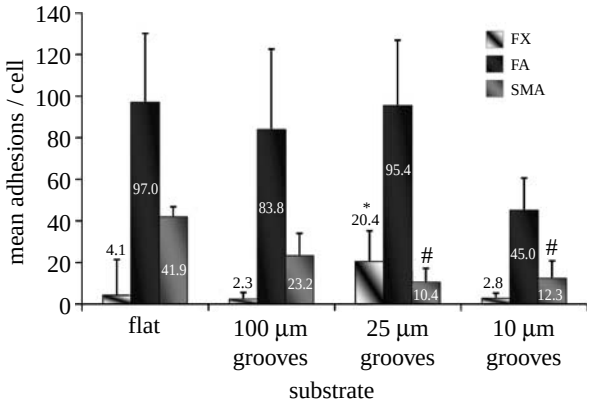

Figure 5. *Quantification of adhesion complex formation in S-phase HOBs on experimental substrates.* SMA formation was greatest in HOBs on planar control substrates, and significantly reduced in cells on 25 and 10 µm grooves. FA incidence was significantly decreased only in HOBs on 10 µm substrates. FX incidence was significantly increased in HOBs on 25 µm grooves. See table 1 for relevant statistics. Included are mean values. Results are mean+s.d.

on both substrates. Adhesion orientation was affected predominantly by 10 µm groove/ridge substrates; here adhesion orientation was largely either parallel or perpendicular to the groove angle (figures 2 and 4*d*).

3.4. Adhesion distribution and quantification

Significant differences in the number of generated adhesion subtypes relative to planar controls were observed on all topographies except the 100 µm groove/ridge arrays. Focal complexes were the least prominent adhesion subtype present in HOBs cultured on planar controls, yet were significantly upregulated in HOBs on 25 µm groove/ridge arrays (figures 5 and 6*a*).

The HOBs on planar controls and 100 µm groove/ridge substrates formed predominantly FA subtypes. The HOBs cultured on planar controls formed on average 97 FAs per cell. This was reduced on both 100 and 25 µm groove/ridge topographies (83.8 and 95.4, respectively) and further reduced on 10 µm groove/ridge topographies (45). Distribution of FAs of greater than 2 µm declined in HOBS on all substrates except planar controls. This was most prominent in HOBs on 25 µm groove/ridge arrays (figures 5 and 6*a*).

Control substrates produced an average of approximately 41.9 SMAs per cell. SMA incidence was reduced on 100 µm groove/ridge arrays (23.2) and significantly reduced on 25 and 10 µm groove/ridge arrays (10.4 and 12.3, respectively). The frequency of SMAs of greater than 8 µm in length was less than 1 per cell in HOBs cultured on 25 and 10 µm groove/ridge arrays. Very large SMAs (greater than 10 µm) were observed only in HOBs cultured on planar control and 100 µm groove/ridge topographies (figures 5 and 6*b*).

3.5. Adhesion orientation

Planar controls, 100 and 25 µm groove/ridge topographies did not significantly affect adhesion orientation. Focal complexes, FAs and SMAs were randomly angled on planar and randomly aligned relative to groove direction on nanotopographies. Adhesion alignment in HOBs cultured on 10 µm groove/ridge arrays was significantly influenced. Here, 20% of all adhesions were parallel with respect to the groove angle (figure 7).

Table 1. *Statistically significant data pertaining to adhesion subtype quantification.* (Kruskal–Wallis one-way analysis of variance was used to estimate the equality of population medians among substrate groups. The largest rank differences were seen between SMA formation on planar and 10 µm groove groups. Data group comparisons indicate a significance of $p<0.05$.)

comparison	difference of ranks
flat SMA versus 10 µm grooves SMA	117.018
flat SMA versus 25 µm grooves SMA	125.878
25 µm groove FX versus 10 µm groove FX	114.578
25 µm groove FX versus 100 µm groove FX	121.862
25 µm groove FX versus flat FX	107.298

3.6. Microarray analysis

Because 10 µm groove/ridge arrays induced the most significant changes relative to planar controls in adhesion profile and the 100 µm groove/ridge arrays induced the least significant changes relative to control substrates in adhesion profile, they were selected for further microarray analysis with Stro+ progentior cells.

3.6.1. Canonical pathway analysis. Analysis of microarray data revealed significant changes in canonical genetic pathways of MSCs cultured on nanogroove substrates (figure 8*a*). Changes in gene expression in MSCs cultured on nanogroove substrates relative to MSCs on planar controls were linked to several well-defined canonical pathways. Significant changes in p38 MAPK signalling were prominent on both substrates. A marked increase in PDGF signalling was observed in MSCs cultured on 100 µm groove/ridge arrays, signalling on 10 µm groove/ridge topographies however was reduced. Integrin signalling was upregulated in MSCs cultured on 100 µm groove/ridge arrays; however, integrin expression was significantly downregulated in MSCs cultured on 10 µm groove/ridge arrays (figure 9*a*,*b*). Significant upregulations were noted in VEGF signalling in cells on 10 µm groove/ridge arrays.

3.6.2. Functional pathway analysis. Nanotopography significantly influenced genetic pathways linked to MSC function (figure 8*b*). Of most significance were large changes in connective tissue development in MSCs cultured on both grooved substrates. Trends indicate enhanced changes occurred in MSCs cultured on 10 µm relative to 100 µm groove/ridge arrays. Cellular movement, proliferation and protein synthesis were all significantly modified in MSCs cultured on 10 µm groove/ridge topographies. Cell morphology was significantly affected on both substrates,

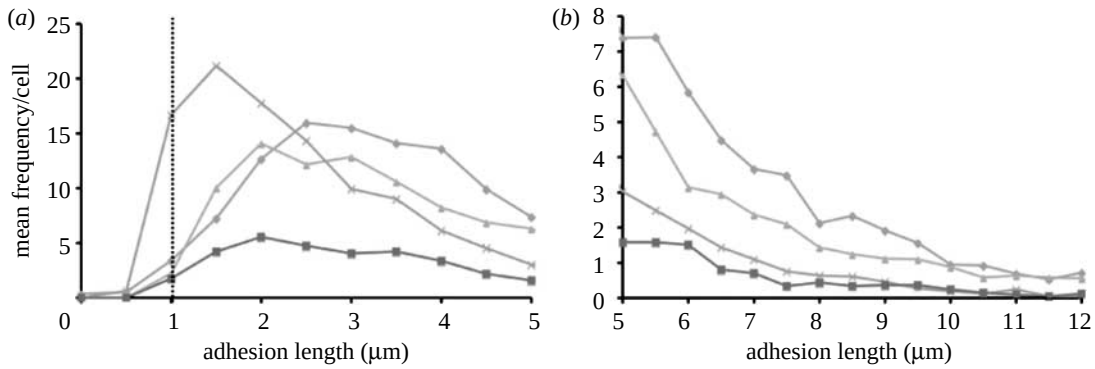

Figure 6. *Adhesion complex distribution in S-phase HOBs on experimental substrates.* (*a*) FXs measuring less than 1 μm in length were most abundant in HOBs on 25 μm grooves. Distribution of FXs approaching 2 μm in length was increased on flat and 100 μm groove substrates. All experimental substrates show a similar decline in adhesion complex distribution as FA lengths approach 4 μm. (*b*) SMAs are most pronounced in HOBs cultured on control substrates. SMA frequency declines on all substrates as length increases (diamonds, flat; triangles, 100 μm grooves; crosses, 25 μm grooves; squares, 10 μm grooves).

correlating with cytoskeletal changes (figures 2, 3 and 8*b*). Significant downregulations in cell proliferation were noted in cells cultured on 10 μm groove/ridge arrays. Upregulation of seven genes fundamental to skeletal system development was noted in HOBs on 100 μm groove/ridge arrays. Only five of these genes were upregulated in HOBs on 10 μm groove/ridge arrays (data not shown).

4. DISCUSSION

Microtopography has been shown in previous studies to be an important mediator of cellular function, regulating cellular adhesion (Hamilton & Brunette 2007), spreading (Biggs *et al.* 2006; Gallant *et al.* 2007) and differentiation (Isa *et al.* 2006) as well as protein adsorption (Sela *et al.* 2007) and soft tissue response (Campbell & Von Recum 1989). While microscale topography significantly modulates cellular behaviour *in vitro*, due to the nanometre size of cellular components concerned with cell–biomaterial interactions, the surface structure of an implanted device influences the cell adhesion processes when the surface topography is within nanometre range (Dalby *et al.* 2003*a*; Cavalcanti-Adam *et al.* 2007; Lim *et al.* 2007). In order to elucidate the effects of topographical cues on primary HOB populations, we used biologically relevant nanoscale substrates to examine cell-substratum adhesion in osteoblasts and the functional response of Stro+ progenitor cells.

Mineralized tissues can be viewed as a dynamic system of self-regulating nanostructures containing grooves and ridges imparted by the collagen and mineral constituents. Previous studies have concluded that the interplay between both groove depth and width modulate cellular response and induce contact guidance (Sutherland *et al.* 2005). We hypothesized that topography with both nano- and microscale dimensions that closely approximate the size of *in vivo* topographical features found in mineralized tissues would better support osteoblast adhesion and MSC function. Loesberg *et al.* (2007) hypothesized that a cellular 'point break' is reached, with decreasing nanogroove width, where cells no longer display contact

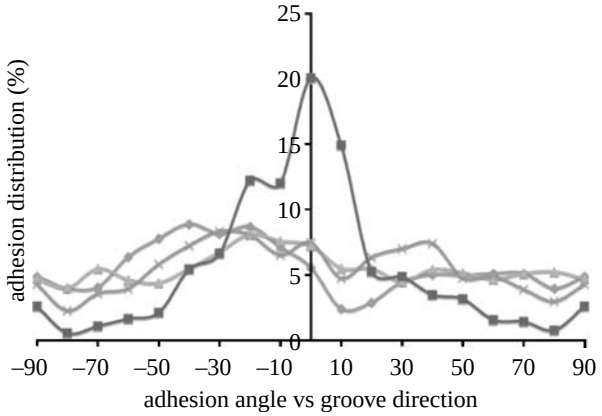

Figure 7. *Adhesion complex alignment on experimental substrates.* Adhesion complex alignment was affected only by 10 μm groove substrates. The majority of adhesions on this topography deviated less than 30° from the groove direction. Approximately 20% of adhesions were aligned parallel with the grooves (diamonds, flat; triangles, 100 μm grooves; crosses, 25 μm grooves; squares, 10 μm grooves).

guidance; this cut-off point was found to be 100 nm in width and 35 nm in depth. A study by Hu *et al.* (2005) also on approximately 300 nm deep grooves concluded that the efficiency of smooth muscle cell alignment and elongation increases monotonically with the decrease of groove pitch, indicating that nanoscale structures produce more efficient alignment and elongation than micrometer-scale patterns. Similarly, we noted an increase in both cellular and adhesion alignment with decreasing groove pitch.

This study used photolithography to create anisotropic topographies of grooves and ridges possessing microscale widths and a constant nanoscale depth. Photolithography fabrication was followed by an embossing process to produce substrates with a constant surface chemistry that exhibited high fidelity from the master templates as well as high reproducibility. No satisfactory conclusions have been reached regarding the elastic properties of bone tissue; however, current literature places the elastic modulus of trabecular bone between 10 and 20 GPa, depending

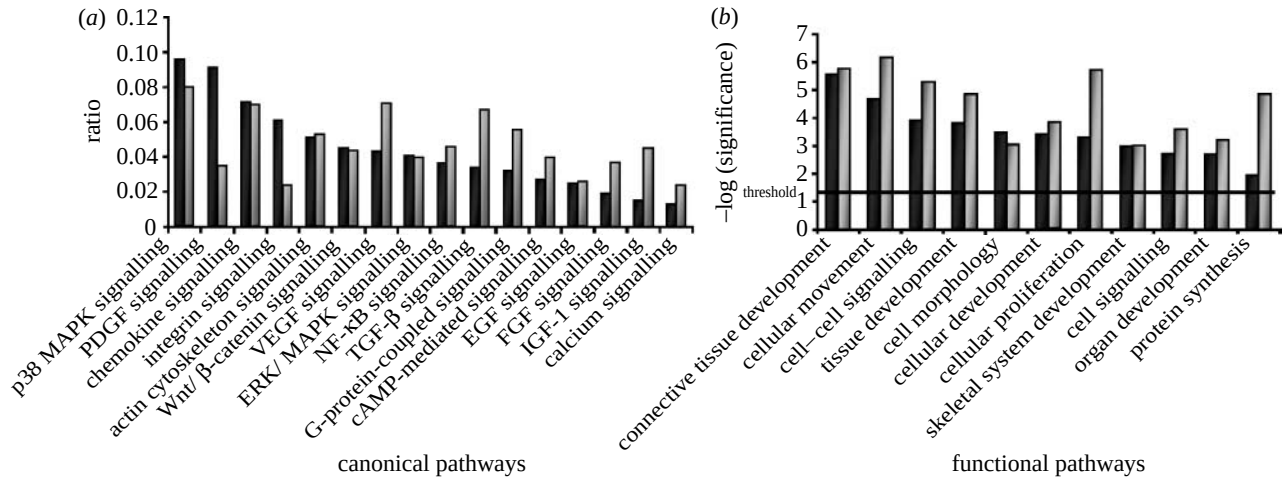

Figure 8. *Ingenuity analysis of Stro+ progenitor cells on experimental substrates.* (*a*) Canonical pathway analysis of Stro+ progenitor cells on experimental substrates identified numerous well-defined signalling pathways that were most affected in cells cultured on groove/ridge substrates. Large changes in p38 MAPK signalling were induced by 100 µm grooves (black bars) while VEGF canonical pathways were most affected by 10 µm grooves (grey bars). Gene expression ratios between experimental and control substrates are indicated. (*b*) The functional analysis of a network of identified biological pathways that were most significant to the genes in the network affected by the groove/ridges. Progenitor cells cultured on both 10 and 100 µm groove nanopit arrays were associated with significant changes in gene expression and function; in particular, connective tissue development and cellular proliferation. A statistical threshold of significance $p=0.05$ indicates the probability that the association between the genes in the dataset canonical pathway is explained by chance alone.

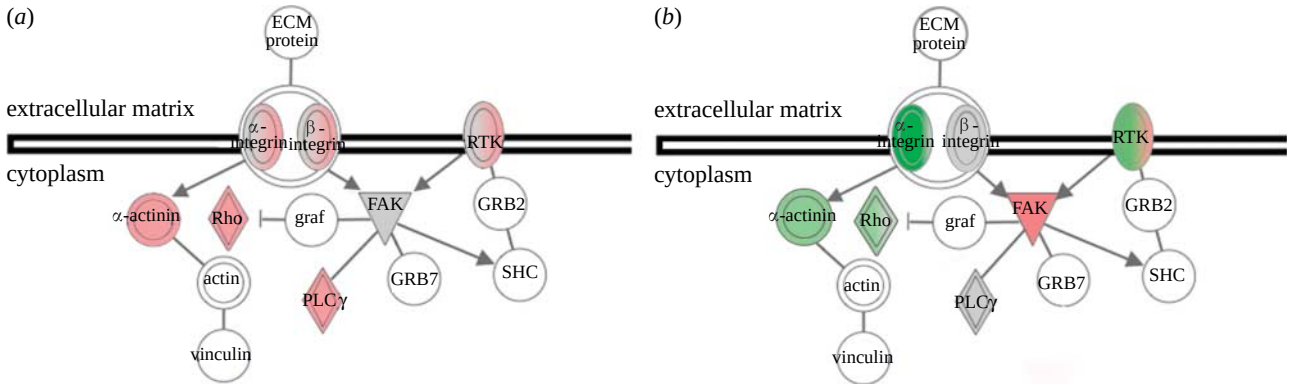

Figure 9. *Integrin signalling in Stro+ progenitor cells on experimental substrates.* (*a*) Expression of genes involved in integrin signalling pathways was upregulated in progenitor cells cultured on 100 µm grooves. (*b*) Downregulations were observed in similar genes in progenitor cells cultured on 10 µm grooves. Red, upregulated; green, downregulated; grey, no change.

on the experimental procedure. To ensure a substrate stiffness comparable with that of trabecular bone, experimental substrates were fabricated in pMMA, an amorphous stiff polymer with an elastic modulus of approximately 3 GPa.

The rationale behind measuring cell adhesions in S-phase HOBs relates to variation in adhesion density measurements that occur as a cell progresses through the cell cycle, and that S-phase cells undergo extreme cell flattening relative to non-S-phase cells that display a more spherical morphology with less cell–substrate contact area (Hunter *et al.* 1995). Meredith *et al.* (2004) previously reported on the low sample variation with respect to adhesion density measurements in S-phase fibroblasts, facilitating accurate adhesion quantification. In this study, changes observed in HOBs cultured on nanogroove substrates were directly linked to the topographical modification, rather than to morphological changes that occur with HOB progression through the cell cycle.

In this study, we characterized vinculin-positive SMAs in primary HOBs on nanogroove and planar substrates. These structures appeared similar to elongated FAs and were prominent in well-spread osteoblasts such as those found on control and 100 µm groove/ridge substrates. We hypothesized that the mechanosensory function of FAs facilitates increased intracellular tension on these substrates and anisotropic protein recruitment at the adhesion plaque resulting in the generation of elongated fibrillar-like adhesions. These SMAs, although morphologically fibrillar, retain the molecular composition of classic FAs including vinculin and FA kinase (FAK; Zamir *et al.* 2000; Cukierman *et al.* 2001). It is probable that the generation of these SMAs and the conservation of FA-associated proteins, most notably FAK, induces increased upregulation in many major signalling pathways.

The S-phase HOBs cultured on planar controls formed predominantly mature FAs and SMAs, indicative of a well-adhered, well-spread phenotype. The HOBs

cultured on experimental substrates demonstrated varying degrees of contact guidance and adhesion formation dependent on groove width. Adhesion complex formation was most perturbed in HOBs cultured on 10 µm groove/ridge arrays. Here, frequency of both FAs and SMAs was reduced. The increased number of focal complexes in HOBs on 25 µm groove/ridge substrates indicates a possible increase in cell motility and filopodia formation, a phenomenon that has been shown to occur on nanoscale topographies previously (Diehl *et al.* 2005). SMAs were significantly reduced in S-phase HOBs on 25 and 10 µm groove/ridge topographies, indicating a reduction in cell adhesion. It has been reported that aligned and elongated fibroblasts on micro- and nanoscale grooves secrete elevated levels of ECM as compared with non-aligned cells (Chou *et al.* 1995; Zhu *et al.* 2005). In this study, a correlation between cellular alignment and increased connective tissue synthesis was noted, supporting the hypothesis that cells dynamically interact with underlying topography and alteration of the ECM is reflected in cell function and behaviour (Adams 2002).

Immuno-SEM revealed adhesion formation of all subtypes to occur predominantly on the top of the ridge structures, a phenomenon previously reported by Teixeira *et al.* (2003). Adhesion to the ridge surface was prevalent in HOBs cultured on 10 and 25 µm groove/ridge arrays (figure 4*c*) but was absent in HOBs on 100 µm groove/ridge topographies, as increased inter-ridge area facilitated increased osteoblast spreading on both ridge and groove areas (figure 4*b*). Groove regions facilitated FA and SMA formation in the direction of groove propagation, aligning both osteoblasts and peripheral adhesions with groove orientation (figure 4*d*). Integrin-mediated adhesion aligning also occurred in the absence of cellular alignment, a phenomenon previously observed only on microgroove topographies (Richards *et al.* 1997). It has been suggested that the geometrical dimensions of the FA plaques force propagation on a grooved surface to be orientated parallel to these ridges (Ohara & Buck 1979). FAs show highly anisotropic growth dynamics in which additional proteins are mostly accumulated in the direction of the force exerted by the cytoskeleton (Besser & Safran 2006). Cellular and cytoskeletal alignment has generally been found to be more pronounced on patterns with ridge widths between 1 and 5 µm than on grooves and ridges with larger lateral dimensions (Matsuzaka *et al.* 2000; Teixeira *et al.* 2003; Karuri *et al.* 2004) such as those used in this study.

Integrin-mediated adhesion plaques act as sites for signal transduction, linking the transcriptional machinery of a cell to its outside environment. Indirect mechanotransductive pathways act to propagate mechanical forces from the ECM to the cell nucleus, regulating cellular response through a dynamic network of protein interaction. It is hypothesized that via direct linkage of the cytoskeletal intermediate filaments to the nucleoskeletal intermediate filaments (lamins) and the association of lamins with the interphase chromosomes, direct linkage from cellular adhesions to DNA is achieved and genomic regulation may thus be controlled by cell adhesion (Dalby 2005; Dalby *et al.* 2006). Indeed, a study by Jean *et al.* (2004) concluded that nuclear deformation appeared to be in direct and immediate response to alterations in cell adhesion area, hence it seems probable that direct mechanotranscriptive pathways play a major role in modulating cellular function in progenitor cells cultured on nanogrooved topographies.

Nanogrooves induced changes in osteoblast cytoskeletal organization, cellular morphology and, primarily, adhesion formation, which were correlated to significant alterations in osteoprogenitor gene expression (figure 9). HOBs cultured on 10 µm groove/ridge arrays demonstrated a downregulation in Rho expression (figure 9*a*), typical in cells undergoing increased cell migration, when focal complexes and lamellapodia are more prominent than FAs and stress fibres (Bershadsky *et al.* 2003). Conversely, this protein was upregulated in Stro+ progenitors cultured on 100 µm groove/ridge arrays (figure 9*b*), typical of well-spread, adhered cells. One of the main downstream targets of Rho is mDia (Riveline *et al.* 2001), a protein that may regulate microtubule polymerization (Schwarz & Bischofs 2005).

Expression of α-actinin was increased in progenitor cells cultured on 100 µm and reduced in cells cultured on 10 µm groove/ridge topographies, a major stress fibre-associated protein that plays a key role in bundling and maintaining the stability of the stress fibres (Byers *et al.* 1984; Burridge *et al.* 1988). In addition to functioning as an organizer of stress fibres, α-actinin also directly connects the stress fibres to FAs via the structural protein vinculin (Katoh *et al.* 2007). A downregulation in α-actinin expression will result in decreased tension-dependent adhesion growth, cellular tension and subsequent adhesion-mediated cellular signalling in cells cultured on 10 µm groove/ridge arrays. It appears that nanogroove substrates act as mediators of cellular function through both the regulation of adhesion formation and subsequent signalling pathways activated/deactivated by cellular elongation.

5. CONCLUSION

Dynamic regulation of FA structure and the integrin–cytoskeleton associations modulating cellular function play a central role in balancing adhesive and migratory stimuli in the cell (Cohen *et al.* 2004). Nanogroove feature dimension influences the generation of adhesion complex subtypes in S-phase HOBs as well as modulates the functional response in Stro+ progenitor populations. Increased groove width is associated with reduced contact guidance and increased adhesion formation and osteospecific function. Conversely, decreased nanogroove widths were associated with increased contact guidance, reduced adhesion formation and an increase in angiospecific function. These findings are intriguing as they indicate that a critical frequency of nanofeatures is necessary to modulate cellular adhesion and subsequent cellular function, and may provide valuable insight for the fabrication of osteoinductive biomaterials with significant clinical implications.

This work was supported by a grant 04-D81 from the AO Research Fund, Switzerland. M.J.D. is a BBSRC David Phillips Fellow and is supported through this fellowship. We would like to acknowledge the work of the Sir Henry Wellcome Functional Genomics Facility and thank the following people: Prof. Adam Curtis and Dr Mathis Riehle for their interesting discussions and support, John Pedersen (SDC Dandisc A/S, Denmark) for the organizing and preparation of nickel shims, Bill Monaghan and Mary Robertson for embossing into pMMA and materials characterization. We also thank Dr Rahul Tare, Bone & Joint Research Group, University of Southampton, for the provision of immunoselected enriched MSC populations and Mrs Pamela Furlong for technical assistance with SEM sample preparation.

REFERENCES

Abercrombie, M., Heaysman, J. E. & Pegrum, S. M. 1971 The locomotion of fibroblasts in culture. IV. Electron microscopy of the leading lamella. *Exp. Cell Res.* **67**, 359–367. (doi:10.1016/0014-4827(71)90420-4)

Adams, J. C. 2002 Molecular organisation of cell–matrix contacts: essential multiprotein assemblies in cell and tissue function. *Expert Rev. Mol. Med.* **4**, 1–24. (doi:10.1017/S1462399402004039)

Bershadsky, A. D., Tint, I. S., Neyfakh Jr, A. A. & Vasiliev, J. M. 1985 Focal contacts of normal and RSV-transformed quail cells. Hypothesis of the transformation-induced deficient maturation of focal contacts. *Exp. Cell Res.* **158**, 433–444. (doi:10.1016/0014-4827(85)90467-7)

Bershadsky, A. D., Balaban, N. Q. & Geiger, B. 2003 Adhesion-dependent cell mechanosensitivity. *Annu. Rev. Cell Dev. Biol.* **19**, 677–695. (doi:10.1146/annurev.cellbio.19.111301.153011)

Bershadsky, A., Kozlov, M. & Geiger, B. 2006 Adhesion-mediated mechanosensitivity: a time to experiment, and a time to theorize. *Curr. Opin. Cell Biol.* **18**, 472–481. (doi:10.1016/j.ceb.2006.08.012)

Besser, A. & Safran, S. A. 2006 Force-induced adsorption and anisotropic growth of focal adhesions. *Biophys. J.* **90**, 3469–3484. (doi:10.1529/biophysj.105.074377)

Biggs, M. J., Richards, R. G., Gadegaard, N., Wilkinson, C. D. & Dalby, M. J. 2006 Regulation of implant surface cell adhesion: characterization and quantification of S-phase primary osteoblast adhesions on biomimetic nanoscale substrates. *J. Orthop. Res.* **25**, 273–282. (doi:10.1002/jor.20319)

Biggs, M. J., Richards, R. G., Gadegaard, N., Wilkinson, C. D. & Dalby, M. J. 2007 The effects of nanoscale pits on primary human osteoblast adhesion formation and cellular spreading. *J. Mater. Sci. Mater. Med.* **18**, 399–404. (doi:10.1007/s10856-006-0705-6)

Bozec, L., De Groot, J., Odlyha, M., Nicholls, B. & Horton, M. A. 2005 Mineralised tissues as nanomaterials: analysis by atomic force microscopy. *IEE Proc. Nanobiotechnol.* **152**, 183–186. (doi:10.1049/ip-nbt:20050004)

Brodsky, B. & Persikov, A. V. 2005 Molecular structure of the collagen triple helix. *Adv. Protein Chem.* **70**, 301–339. (doi:10.1016/S0065-3233(05)70009-7)

Burridge, K., Fath, K., Kelly, T., Nuckolls, G. & Turner, C. 1988 Focal adhesions: transmembrane junctions between the extracellular matrix and the cytoskeleton. *Annu. Rev. Cell Biol.* **4**, 487–525. (doi:10.1146/annurev.cb.04.110188.002415)

Byers, H. R., White, G. E. & Fujiwara, K. 1984 Organization and function of stress fibers in cells *in vitro* and *in situ*. A review. *Cell Muscle Motil.* **5**, 83–137.

Campbell, C. E. & Von Recum, A. F. 1989 Microtopography and soft tissue response. *J. Invest. Surg.* **2**, 51–74. (doi:10.3109/08941938909016503)

Cavalcanti-Adam, E. A., Volberg, T., Micoulet, A., Kessler, H., Geiger, B. & Spatz, J. P. 2007 Cell spreading and focal adhesion dynamics are regulated by spacing of integrin ligands. *Biophys. J.* **92**, 2964–2974. (doi:10.1529/biophysj.106.089730)

Chou, L., Firth, J. D., Uitto, V. J. & Brunette, D. M. 1995 Substratum surface topography alters cell shape and regulates fibronectin mRNA level, mRNA stability, secretion and assembly in human fibroblasts. *J. Cell Sci.* **108**(Pt 4), 1563–1573.

Cohen, M., Joester, D., Geiger, B. & Addadi, L. 2004 Spatial and temporal sequence of events in cell adhesion: from molecular recognition to focal adhesion assembly. *Chembiochem* **5**, 1393–1399. (doi:10.1002/cbic.200400162)

Cukierman, E., Pankov, R., Stevens, D. R. & Yamada, K. M. 2001 Taking cell–matrix adhesions to the third dimension. *Science* **294**, 1708–1712. (doi:10.1126/science.1064829)

Curtis, A. S. 1964 The mechanism of adhesion of cells to glass. A study by interference reflection microscopy. *J. Cell Biol.* **20**, 199–215. (doi:10.1083/jcb.20.2.199)

Dalby, M. J. 2005 Topographically induced direct cell mechanotransduction. *Med. Eng. Phys.* **27**, 730–742. (doi:10.1016/j.medengphy.2005.04.005)

Dalby, M. J., Riehle, M. O., Johnstone, H. J., Affrossman, S. & Curtis, A. S. 2003*a* Nonadhesive nanotopography: fibroblast response to poly(*n*-butyl methacrylate)-poly(styrene) demixed surface features. *J. Biomed. Mater. Res. A* **67**, 1025–1032. (doi:10.1002/jbm.a.10139)

Dalby, M. J., Riehle, M. O., Yarwood, S. J., Wilkinson, C. D. & Curtis, A. S. 2003*b* Nucleus alignment and cell signaling in fibroblasts: response to a micro-grooved topography. *Exp. Cell Res.* **284**, 274–282. (doi:10.1016/S0014-4827(02)00053-8)

Dalby, M. J., Riehle, M. O., Sutherland, D. S., Agheli, H. & Curtis, A. S. 2005 Morphological and microarray analysis of human fibroblasts cultured on nanocolumns produced by colloidal lithography. *Eur. Cell Mater.* **9**, 1–8.

Dalby, M. J., Biggs, M. J., Gadegaard, N., Kalna, G., Wilkinson, C. D. & Curtis, A. S. 2006 Nanotopographical stimulation of mechanotransduction and changes in interphase centromere positioning. *J. Cell Biochem.* **100**, 326–338. (doi:10.1002/jcb.21058)

Den Braber, E. T., De Ruijter, J. E., Ginsel, L. A., Von Recum, A. F. & Jansen, J. A. 1998 Orientation of ECM protein deposition, fibroblast cytoskeleton, and attachment complex components on silicone microgrooved surfaces. *J. Biomed. Mater. Res.* **40**, 291–300. (doi:10.1002/(SICI)1097-4636(199805)40:2<291::AID-JBM14>3.0.CO;2-P)

Diehl, K. A., Foley, J. D., Nealey, P. F. & Murphy, C. J. 2005 Nanoscale topography modulates corneal epithelial cell migration. *J. Biomed. Mater. Res. A* **75**, 603–611. (doi:10.1002/jbm.a.30467)

Gadegaard, N., Mosler, M. & Larsen, M. B. 2003 Biomimetic polymer nanostructures by injection molding. *Macromol. Mater. Eng.* **288**, 76–83. (doi:10.1002/mame.200290037)

Gallant, N. D., Charest, J. L., King, W. P. & Garcia, A. J. 2007 Micro- and nano-patterned substrates to manipulate cell adhesion. *J. Nanosci. Nanotechnol.* **7**, 803–807. (doi:10.1166/jnn.2007.507)

Giraud-Guille, M. M. 1988 Twisted plywood architecture of collagen fibrils in human compact bone osteons. *Calcif. Tissue Int.* **42**, 167–180. (doi:10.1007/BF02556330)

Hamilton, D. W. & Brunette, D. M. 2007 The effect of substratum topography on osteoblast adhesion mediated signal transduction and phosphorylation. *Biomaterials* **28**, 1806–1819. (doi:10.1016/j.biomaterials.2006.11.041)

Howard, D., Partridge, K., Yang, X., Clarke, N. M., Okubo, Y., Bessho, K., Howdle, S. M., Shakesheff, K. M. & Oreffo, R. O. 2002 Immunoselection and adenoviral genetic modulation of human osteoprogenitors: *in vivo* bone formation on PLA scaffold. *Biochem. Biophys. Res. Commun.* **299**, 208–215. (doi:10.1016/S0006-291X(02)02561-5)

Hu, W., Yim, E. K. F., Reano, R. M., Leong, K. W. & Pang, S. W. 2005 Effects of nanoimprinted patterns in tissue-culture polystyrene on cell behavior. *J. Vasc. Sci. Technol. B* **23**, 2984–2989. (doi:10.1116/1.2121729)

Hunter, A., Archer, C. W., Walker, P. S. & Blunn, G. W. 1995 Attachment and proliferation of osteoblasts and fibroblasts on biomaterials for orthopaedic use. *Biomaterials* **16**, 287–295. (doi:10.1016/0142-9612(95)93256-D)

Isa, Z. M., Schneider, G. B., Zaharias, R., Seabold, D. & Stanford, C. M. 2006 Effects of fluoride-modified titanium surfaces on osteoblast proliferation and gene expression. *Int. J. Oral Maxillofac. Implants* **21**, 203–211.

Jean, R. P., Gray, D. S., Spector, A. A. & Chen, C. S. 2004 Characterization of the nuclear deformation caused by changes in endothelial cell shape. *J. Biomech. Eng.* **126**, 552–558. (doi:10.1115/1.1800559)

Karuri, N. W., Liliensiek, S., Teixeira, A. I., Abrams, G., Campbell, S., Nealey, P. F. & Murphy, C. J. 2004 Biological length scale topography enhances cell-substratum adhesion of human corneal epithelial cells. *J. Cell Sci.* **117**, 3153–3164. (doi:10.1242/jcs.01146)

Katoh, K., Kano, Y. & Ookawara, S. 2007 Rho-kinase dependent organization of stress fibers and focal adhesions in cultured fibroblasts. *Genes Cells* **12**, 623–638. (doi:10.1111/j.1365-2443.2007.01073.x)

Lenhert, S., Meier, M. B., Meyer, U., Chi, L. & Wiesmann, H. P. 2005 Osteoblast alignment, elongation and migration on grooved polystyrene surfaces patterned by Langmuir–Blodgett lithography. *Biomaterials* **26**, 563–570. (doi:10.1016/j.biomaterials.2004.02.068)

Lim, J. Y., Dreiss, A. D., Zhou, Z., Hansen, J. C., Siedlecki, C. A., Hengstebeck, R. W., Cheng, J., Winograd, N. & Donahue, H. J. 2007 The regulation of integrin-mediated osteoblast focal adhesion and focal adhesion kinase expression by nanoscale topography. *Biomaterials* **28**, 1787–1797. (doi:10.1016/j.biomaterials.2006.12.020)

Loesberg, W. A., Te Riet, J., Van Delft, F. C., Schon, P., Figdor, C. G., Speller, S., Van Loon, J. J., Walboomers, X. F. & Jansen, J. A. 2007 The threshold at which substrate nanogroove dimensions may influence fibroblast alignment and adhesion. *Biomaterials* **28**, 3944–3951. (doi:10.1016/j.biomaterials.2007.05.030)

Matsuzaka, K., Walboomers, F., De Ruijter, A. & Jansen, J. A. 2000 Effect of microgrooved poly-l-lactic (PLA) surfaces on proliferation, cytoskeletal organization, and mineralized matrix formation of rat bone marrow cells. *Clin. Oral Implants Res.* **11**, 325–333. (doi:10.1034/j.1600-0501.2000.011004325.x)

Meredith, D. O., Owen, G. R., Ap Gwynn, I. & Richards, R. G. 2004 Variation in cell-substratum adhesion in relation to cell cycle phases. *Exp. Cell Res.* **293**, 58–67. (doi:10.1016/j.yexcr.2003.10.005)

Mirmalek-Sani, S. H., Tare, R. S., Morgan, S. M., Roach, H. I., Wilson, D. I., Hanley, N. A. & Oreffo, R. O. 2006 Characterization and multipotentiality of human fetal femur-derived cells: implications for skeletal tissue regeneration. *Stem Cells* **24**, 1042–1053. (doi:10.1634/stemcells.2005-0368)

Ohara, P. T. & Buck, R. C. 1979 Contact guidance *in vitro*. A light, transmission, and scanning electron microscopic study. *Exp. Cell Res.* **121**, 235–249. (doi:10.1016/0014-4827(79)90002-8)

Rho, J. Y., Kuhn-Spearing, L. & Zioupos, P. 1998 Mechanical properties and the hierarchical structure of bone. *Med. Eng. Phys.* **20**, 92–102. (doi:10.1016/S1350-4533(98)00007-1)

Richards, R. G. & Ap Gwynn, I. 1995 Backscattered electron imaging of the undersurface of resin-embedded cells by field emission scanning electron microscopy. *J. Microsc.* **177**, 43–52.

Richards, R. G., Rahn, B. A. & Ap Gwynn, I. 1997 A quantitative method of measuring cell adhesion areas. Review. *Cells Mater.* **7**, 15–30.

Richards, R. G., Stiffanic, M., Owen, G. R., Riehle, M., Ap Gwynn, I. & Curtis, A. S. 2001 Immunogold labelling of fibroblast focal adhesion sites visualised in fixed material using scanning electron microscopy, and living, using internal reflection microscopy. *Cell Biol. Int.* **25**, 1237–1249. (doi:10.1006/cbir.2001.0807)

Riveline, D., Zamir, E., Balaban, N. Q., Schwarz, U. S., Ishizaki, T., Narumiya, S., Kam, Z., Geiger, B. & Bershadsky, A. D. 2001 Focal contacts as mechanosensors: externally applied local mechanical force induces growth of focal contacts by an mDia1-dependent and ROCK-independent mechanism. *J. Cell Biol.* **153**, 1175–1186. (doi:10.1083/jcb.153.6.1175)

Rubin, M. A., Rubin, J. & Jasiuk, I. 2004 SEM and TEM study of the hierarchical structure of C57BL/6J and C3H/HeJ mice trabecular bone. *Bone* **35**, 11–20. (doi:10.1016/j.bone.2004.02.008)

Schwarz, U. S. & Bischofs, I. B. 2005 Physical determinants of cell organization in soft media. *Med. Eng. Phys.* **27**, 763–772. (doi:10.1016/j.medengphy.2005.04.007)

Sela, M. N., Badihi, L., Rosen, G., Steinberg, D. & Kohavi, D. 2007 Adsorption of human plasma proteins to modified titanium surfaces. *Clin. Oral Implants Res.* **18**, 630–638. (doi:10.1111/j.1600-0501.2007.01373.x)

Sutherland, J., Denyer, M. & Britland, S. 2005 Contact guidance in human dermal fibroblasts is modulated by population pressure. *J. Anat.* **206**, 581–587. (doi:10.1111/j.1469-7580.2005.00415.x)

Teixeira, A. I., Abrams, G. A., Bertics, P. J., Murphy, C. J. & Nealey, P. F. 2003 Epithelial contact guidance on well-defined micro- and nanostructured substrates. *J. Cell Sci.* **116**, 1881–1892. (doi:10.1242/jcs.00383)

Wagner, H. D. & Weiner, S. 1992 On the relationship between the microstructure of bone and its mechanical stiffness. *J. Biomech.* **25**, 1311–1320. (doi:10.1016/0021-9290(92)90286-A)

Zamir, E. & Geiger, B. 2001 Molecular complexity and dynamics of cell–matrix adhesions. *J. Cell Sci.* **114**, 3583–3590.

Zamir, E. *et al.* 2000 Dynamics and segregation of cell–matrix adhesions in cultured fibroblasts. *Nat. Cell Biol.* **2**, 191–196. (doi:10.1038/35008607)

Zhu, B., Lu, Q., Yin, J., Hu, J. & Wang, Z. 2005 Alignment of osteoblast-like cells and cell-produced collagen matrix induced by nanogrooves. *Tissue Eng.* **11**, 825–834. (doi:10.1089/ten.2005.11.825)

Zimerman, B., Volberg, T. & Geiger, B. 2004 Early molecular events in the assembly of the focal adhesion–stress fiber complex during fibroblast spreading. *Cell Motil. Cytoskeleton* **58**, 143–159. (doi:10.1002/cm.20005)